Dilution in Single Pass Arc Welds

J.N. DuPONT and A.R. MARDER

A study was conducted on dilution of single pass arc welds of type 308 stainless steel filler metal deposited onto A36 carbon steel by the plasma arc welding (PAW), gas tungsten arc welding (GTAW), gas metal arc welding (GMAW), and submerged are welding (SAW) processes. Knowledge of the arc and melting efficiency was used in a simple energy balance to develop an expression for dilution as a function of welding variables and thermophysical properties of the filler metal and substrate. Comparison of calculated and experimentally determined dilution values shows the approach provides reasonable predictions of dilution when the melting efficiency can be accurately predicted. The conditions under which such accuracy is obtained are discussed. A diagram is developed from the dilution equation which readily reveals the effect of processing parameters on dilution to aid in parameter optimization.

I. INTRODUCTION

THE weld deposit which develops during fusion welding of two dissimilar alloys will attain a chemical composition intermediate to the two alloys. The final deposit composition will depend on the individual compositions of the materials and the degree of mixing between the alloys. Figure 1 shows this schematically in the simplest form, where a single pass of a filler alloy is deposited onto a substrate of a different composition. The degree of mixing for the simple case illustrated is defined by the percentage dilution, D:

$$\text{Pct } D = \frac{A_s}{A_s + A_{fm}} \times 100 \qquad [1]$$

where A_s is the melted cross-sectional area of the substrate and A_{fm} is the cross-sectional area of the deposited filler metal. The weld deposit composition can be determined if the dilution is known along with the filler metal and substrate compositions. This approach assumes sufficient mixing occurs in the liquid state so that composition gradients are not formed in the weld deposit. Previous work[1,2] has shown that concentration gradients in dissimilar metal welds typically exist only near the fusion line over distances on the order of a few hundred microns. (This discussion does not deal with the relatively small scale concentration gradients in the weld metal which result from solidification segregation.) We provide some additional evidence which supports this claim in a later section. In cases where concentration gradients are insignificant, Eq. [1] can be used to determine the weld deposit composition accurately. Even when composition gradients exist over the entire deposit, knowledge of the dilution permits an estimation of the weld metal composition. Last, it should be noted that Eq. [1] assumes that losses by evaporation are negligible, which may not always be the case for alloying elements which have a high vapor pressure (*e.g.*, Mg in Al alloys[3]).

Control of dilution can be important in dissimilar metal welding applications. In cladding, where a corrosion resistant filler metal is deposited on a less corrosion resistant material, a low dilution is typically desirable. With a low dilution value, the final deposit composition is close to that of the filler metal and the corrosion resistance of the cladding is maintained. Dilution is also important to avoid undesirable phase formation, most notably in joining of ferritic steels to austenitic stainless steels.[4] Despite the importance of dilution, relatively little work has been published which defines, in a quantitative manner, the role of material properties and processing parameters on dilution. Chandel[5] derived empirical equations for A_s and A_{fm} as a function of the welding parameters in order to predict dilution of bead-on-plate welds on carbon steel deposited by the submerged arc welding (SAW) process. Dilution values from 20 to 80 pct were produced, and the empirical equations were found to provide a good prediction of experimentally measured dilution. Oh *et al.*[6] proposed a similar approach based on empirical relations for the electroslag welding process. Although empirical approaches provide a method for estimating dilution, they typically apply only under conditions for which they were derived and do not provide any physical basis to understand the role of processing parameters.

At the other extreme, more recent work[7–10] has been conducted to predict weld pool melt volumes by solving the conservation equations of mass, momentum, and energy computationally which may, eventually, be utilized to calculate weld metal dilution. Although this approach incorporates all the pertinent physical conditions, the dominant physics can often be lost in the complexity of the problem, rendering the approach difficult to utilize for engineering applications. In this work, we take an intermediate approach and develop a simple analytical expression for dilution as a function of welding variables and thermophysical properties of the filler metal and substrate by making use of thermal efficiency factors (arc efficiency and melting efficiency) which were measured and discussed in a previous article[11] for the plasma arc welding (PAW), gas tungsten arc welding (GTAW), gas metal arc welding (GMAW), and submerged arc welding (SAW) processes. The expression applies only to the simple single pass condition illustrated schematically in Figure 1. Effects of multiple, overlapping passes are not considered. Comparison of calculated dilu-

J.N. DuPONT, Associate Research Scientist, and A.R. MARDER, Professor, are with the Department of Materials Science and Engineering, Lehigh University, Bethlehem, PA 18015.

Manuscript submitted October 10, 1995.

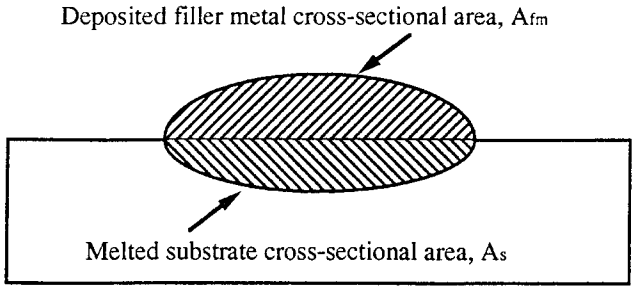

Fig. 1—Schematic illustration of dilution in single pass welds.

tion values to those measured experimentally shows that the approach correctly captures the main factors which affect dilution.

II. EXPERIMENTAL PROCEDURE

Estimation of dilution with the approach presented here requires knowledge of the thermal efficiency (arc efficiency and melting efficiency) of the welding process. The methods and equipment utilized for measuring these thermal efficiency factors have been discussed in detail in a separate article.[11] The welding processes evaluated included PAW, GTAW, GMAW, and SAW. The thermal efficiency factors were determined under the same range of parameters used throughout the present discussion (Table I).

A fully automated welding system designed specifically for research was used for all the experiments. A 500 A constant current/constant voltage power source was used for each process. A separate plasma console unit was used for control of the pilot arc, plasma gas, and shielding gas for the PAW process. Motion of the individual torches was provided by an automated travel carriage. The power source, travel carriage, and all auxiliary equipment are controlled by a Texas Instruments/Siemens programmable control unit.

To simulate the simple dilution condition illustrated schematically in Figure 1, single pass welds were prepared by depositing type 308 austenitic stainless steel onto 305-mm-square by 6.4-mm-thick A36 steel substrate under the range of parameters listed in Table I. (It should be noted that for the GMAW and SAW processes, welding current is controlled mainly by filler metal feed rate. Thus, these variables are not independently controlled.) Each deposit was approximately 254 mm in length. The ranges listed in Table I for each process were determined by preliminary weld trials. The lower limit to travel speed for a given arc power was governed by the formation of excessively wide and deeply penetrating welds. The upper limit of travel speed was established for a given arc power when the process could no longer adequately melt the substrate and filler metal.

The PAW and GTAW processes were conducted using direct current electrode negative (DCEN) polarity with a 4-mm-diameter 2 pct thoriated tungsten electrode and argon shielding gas. The PAW torch was designed specifically for surfacing applications. A large constricting nozzle was used which contained two ports adjacent to the constricting chamber for delivery of type 308 stainless steel powder filler metal into the weld pool. The powder filler metal was fluidized in an argon gas and delivered to the outside ports of the constricting nozzle by a calibrated screw feeder. The stand-off distance was held constant at 15 mm. Argon plasma gas was used at a flow rate of 1 L/min. With the GTAW process, a cold wire feeder supplied a 1.14-mm-diameter 308 austenitic stainless filler wire to the weld pool and the electrode-to-work distance was held constant at 6 mm.

The GMAW and SAW processes were conducted using direct current electrode positive (DCEP) polarity with a 1.14-mm-diameter 308 austenitic stainless steel filler wire. Argon shielding gas was used for the GMAW process. The contact tip-to-work distance of the GMAW process was adjusted for each current and voltage setting to produce a nominal stick-out length of 12 mm. The stick-out length of the SAW process was not controlled due to the inability to observe the arc and electrode. Instead, the contact tip-to-work distance was held constant at 15 mm. For each process, the voltage was measured between the torch and substrate with a programmable voltmeter. The measured voltage represents the sum of voltage drops across the electrode and arc. Current was measured by a calibrated shunt placed in series with the current carrying cable.

After welding, each sample was cross sectioned using an abrasive cutoff wheel, polished to a 1-μm finish using silicon carbide paper, and etched in a 2 pct Nital solution. The individual cross-sectional areas of the melted substrate (A_s) and deposited filler metal (A_{fm}) were then measured using a LECO* quantitative image analysis system. The dilution was determined for each sample by Eq. [1]. One weld deposited by the GMAW process was also mounted and polished to a 0.04-μm finish using colloidal silica for examination by electron probe microanalysis to examine the distribution of alloying elements in the deposit. The profile was obtained on a JEOL** 733 SuperProbe operated at 15 kV and 20 nA beam current. The profile was initiated on the substrate near the bottom of the weld and progressed toward the weld surface. The K_α lines were utilized for all elements analyzed and raw counting data were converted to weight percentages by the ZAF correction scheme. The error in the data was estimated to be ≈2 pct relative.

*LECO is a trademark of LECO Corporation, St. Joseph, MI.

**JEOL is a trademark of Japan Electron Optics Ltd., Tokyo.

III. BACKGROUND

A. *Thermal Efficiency Factors*

As previously noted, estimation of dilution with the approach presented here requires knowledge of the thermal efficiency of the welding process. Thermal efficiency factors for the present set of conditions have been measured and discussed in a separate article.[11] The results will be summarized here, along with a brief discussion on the parameters affecting thermal efficiency factors, to support the background discussion. The term thermal efficiency describes the welding process in two ways, namely, arc efficiency and melting efficiency. Arc efficiency is the fraction of total process energy which is actually delivered to the substrate and weld deposit. The ratio of energy used for

Table I. Experimental Matrix of Processing Parameter Ranges Used in Dilution and Thermal Efficiency Measurements

Process	Current (A)	Voltage (V)	Travel Speed (mm/s)	Filler Metal Feed Rate (mm^3/s)
PAW	250 to 400	25 to 32	2 to 4	8 to 120
GTAW	250 to 400	15 to 16	6 to 10	20 to 130
GMAW	230 to 400	27 to 36	6 to 26	120 to 245
SAW	200 to 330	34 to 37	6 to 26	120 to 245

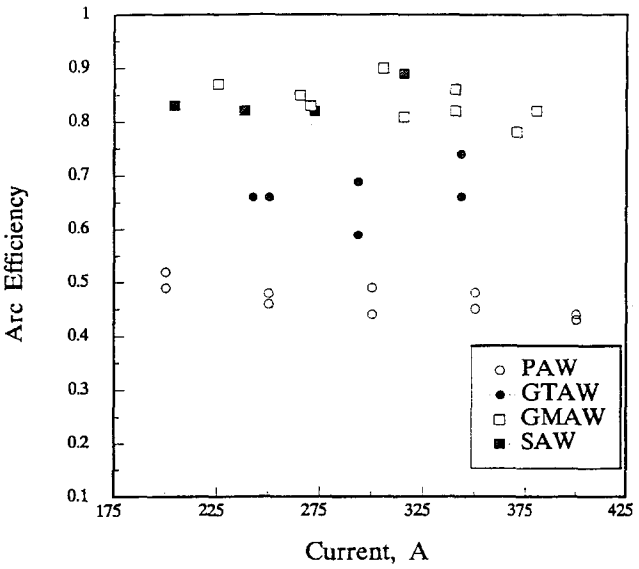

Fig. 2—Arc efficiency as a function of current for the PAW, GTAW, GMAW, and SAW processes.

melting to that which is delivered to the workpiece defines the melting efficiency.

Figure 2 shows the arc efficiency for each welding process considered as a function of welding current. These measurements were conducted using a Seebeck arc welding calorimeter as first described for arc efficiency measurements by Giedt *et al.*[12] A clear distinction in the ability of each process to transfer energy to the workpiece is evident in Figure 2. The data also show there is very little variation in arc efficiency for a given process over the current range investigated. The consumable electrode processes (GMAW and SAW) exhibit an average arc efficiency of 0.84 ± 0.04. The GTAW process has an average arc efficiency of 0.67 ± 0.05, and the PAW process displays an average arc efficiency of 0.47 ± 0.03. These values are in good agreement with other arc efficiencies reported in the literature for these processes.[13,14] Thus, the arc efficiency for a given process under the broad range of current considered can be estimated reasonably well as a constant.

Unlike arc efficiency, the melting efficiency depends strongly on the processing parameters, base metal properties, and base metal thickness. Using the solution derived by Rosenthal for two-dimensional conduction heat flow conditions,[15] Wells[16] provided the first analytical expression for melting efficiency, η_m, in terms of the processing parameters and base metal thermophysical properties:

$$\eta_m = \frac{1}{\frac{8\alpha}{5Sd} + 2} \quad [2]$$

Here, α is the base metal thermal diffusivity, S is the welding speed, and d is the weld width. Okada[17] proposed a similar relation for three-dimensional heat flow conditions:

$$\eta_m = \frac{1}{1.35\left[1 + \left(1 + \frac{10.4\alpha^2}{(Sd)^2}\right)^{1/2}\right]} \quad [3]$$

These relations account for the rapid increase in melting efficiency with travel speed and the saturation of η_m to a value of approximately 0.48 for two-dimensional heat flow and 0.37 for three-dimensional heat flow at high travel speeds when the ratio of thermal diffusivity to travel speed is low, which has been observed experimentally.[11,16,18-20] The relations also reveal the effect of thermal diffusivity, where higher thermal diffusivities promote lower melting efficiencies since heat can be conducted away from the fusion zone quicker. Last, the effect of base metal thickness is demonstrated by the differences between Eq. [2] and [3]. At equivalent travel speeds and thermal diffusivities, melting efficiency is always higher for thin plates which result in two-dimensional heat flow conditions (Eq. [2]) compared to thick plates which promote three-dimensional heat flow conditions (Eq. [3]). In terms of processing parameter effects, Eq. [2] and [3] suggest that travel speed controls the melting efficiency. However, attempts to quantitatively correlate the melting efficiency exclusively to travel speed (for a given material) have generally been unsuccessful.[11,18]

Okada[17] proposed that melting efficiency should depend on the product of net arc power and travel speed and presented a relation of the form

$$\eta_m = \exp - \left(1 + \frac{\alpha^2 E}{1.14\ \eta_a\ VIS}\right) \quad [4]$$

where E is the enthalpy change due to melting, η_a is the arc efficiency, and $\eta_a VI$ is the net arc power delivered to the base metal (V is voltage and I is current). $\eta_a VIS$ represents the product of net arc power and travel speed. In terms of welding variables, the $\eta_a VIS$ parameter has been shown to correlate very well with melting efficiency.[11,18] Although Okada's relation provides a refinement to Eqs. [2] and [3] by correctly identifying the welding parameters which affect melting efficiency (arc power and travel speed), the parameter $\eta_a VIS/\alpha^2 E$ appearing in Eq. [4] is unable to normalize differences in base metal thermophysical properties.[18] More recently, Fuerschbach and Knorovsky[18] have demonstrated that melting efficiency can be estimated from the welding parameters and material properties by an equation of the form

$$\eta_m = A \exp\left(\frac{-B}{\eta_a VIS\ /\ E\alpha\nu}\right) \quad [5]$$

Here, α is the thermal diffusivity at 300 K and ν is the kinematic viscosity at the melting point. The quantity ($\eta_a VIS/E\alpha\nu$) is a dimensionless parameter. The constant A is representative of the maximum melting efficiency for a given joint design or substrate geometry which is obtained

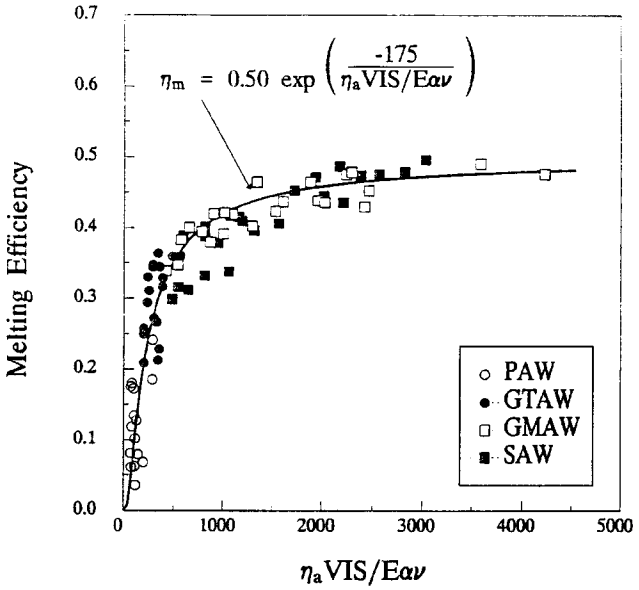

Fig. 3—Variation in melting efficiency with the $\eta_a VIS/E\alpha\nu$ parameter for the PAW, GTAW, GMAW, and SAW processes.

when the quantity $(\eta_a VIS/E\alpha\nu)$ is large. The constants A and B can be determined from the intercept (A) and slope (B) on a plot of ln (η_m) against $(\eta_a VIS/E\alpha\nu)^{-1}$.

Figure 3 shows melting efficiency plotted against this dimensionless parameter for the present set of conditions. An average value between carbon steel and austenitic stainless steel of $E = 9.6$ J mm^{-3}[21,22] and $\nu = 0.84$ mm^2 s^{-1} [23] was used in the plot. The effect of thermal diffusivity should be controlled by the substrate, so the value for steel was used (9.1 mm^2 s^{-1} [24]). With these values, $E\alpha\nu = 73$ J mm s^{-2}. Since the substrate and filler metal are held constant in this experiment and the value of $E\alpha\nu$ is therefore fixed, the plot of the data using this dimensionless parameter does not provide an opportunity to reveal the effectiveness of the parameter to normalize the influence of material property variations. However, it does reveal the proper dependence of melting efficiency on the process parameters (arc power and travel speed). In addition, this parameter has been shown to normalize differences in material thermophysical properties between 304 stainless steel and NI 200 in an edge weld configuration.[18] The approach is adopted here to facilitate prediction of the melting efficiency in order to estimate the dilution. Equation [5] is plotted in Figure 3 with the constants $A = 0.50$ and $B = 175$, and the expression provides a reasonable representation of the experimental data. Thus, in terms of the thermal efficiency factors, the arc efficiency is approximately constant for a given process under a broad range of current, while the melting efficiency can be estimated *via* Eq. [5], where A and B are experimentally determined constants. Under the present conditions, where single pass welds of 308 stainless steel are deposited on 6.4-mm-thick A36 steel substrate, $A = 0.50$ and $B = 175$.

B. *Estimating Dilution*

When dilution is determined by metallographic methods, it is typically calculated by the individual cross-sectional area terms of the deposited filler metal and melted substrate, as given by Eq. [1]. However, dilution is actually the result of the volumetric quantities v_{fm} and v_s, where v_{fm} is the volume of deposited filler metal and v_s is the volume of melted substrate. These volumetric terms are simply reduced by one dimension into an area term when the sample is cross sectioned and the measurements of A_s and A_{fm} are made, the assumption being that the cross-sectional areas do not vary along the length of the sample. Constant cross-sectional areas are produced along the weld length when the volumetric melting rate of the filler metal, V_{fm}, and the substrate, V_s, are constant with travel speed. Under this assumption, dilution can also be expressed in terms of the volumetric melting rates of the substrate and the filler metal:

$$\text{Pct } D = \left(\frac{V_s}{V_s + V_{fm}}\right) \times 100 \qquad [6]$$

The volumetric melting rate of the filler metal is a controlled variable of the process. The implicit assumption in using the *set* value of volumetric filler metal feed rate to represent the *actual deposited* volumetric filler metal rate is that filler metal losses due to spatter are negligible. An expression for V_s can be obtained by considering a simplified balance of power terms across the welding arc which is facilitated by the thermal efficiency factors.

$$\eta_a \eta_m VI = V_{fm}\left(\int Cp\,(T)\,dT + \Delta H_f\right)_{fm} + V_s\left(\int Cp\,(T)\,dT + \Delta H_f\right)_s \qquad [7]$$

The $(\int C_p(T)dT + \Delta H_f)_{fm}$ and $(\int C_p(T)dT + \Delta H_f)_s$ terms (C_p is specific heat and ΔH_f is latent heat of fusion) represent the enthalpy change required to melt a given volume of filler metal and substrate. These terms can be represented by E_{fm} for the filler metal and E_s for the substrate for simplicity. The values for these thermophysical properties under the present conditions are $E_{fm} = 8.7$ J mm^{-3} [22] for type 308 stainless steel and $E_s = 10.5$ J mm^{-3} [21] for carbon steel. The left side of Eq. [7] represents the melting power delivered by the arc, while the right side represents the power required for melting of the substrate and filler metal. Equation [7] can be rewritten in simpler form:

$$\eta_a \eta_m VI = V_{fm}E_{fm} + V_s E_s \qquad [8]$$

The arc and melting efficiencies can be estimated, as discussed in Section A. Thus, V_s is the only unknown in Eq. [8]. Rearranging Eq. [8], we obtain

$$V_s = \frac{\eta_a \eta_m VI - V_{fm}E_{fm}}{E_s} \qquad [9]$$

Writing Eq. [6] in a more convenient form gives

$$\text{Pct } D = \left(1 + \frac{V_{fm}}{V_s}\right)^{-1} \times 100 \qquad [10]$$

and substituting Eq. [9] into Eq. [10], an equation for dilution can be obtained:

$$\text{Pct } D = \left[1 + \frac{V_{fm}E_s}{\eta_a \eta_m VI - E_{fm}V_{fm}}\right]^{-1} \times 100 \qquad [11]$$

Equation [11] provides an analytical expression for dilution in terms of the welding parameters which are controlled during the process, thermal efficiency factors which can be estimated as previously discussed, and filler metal

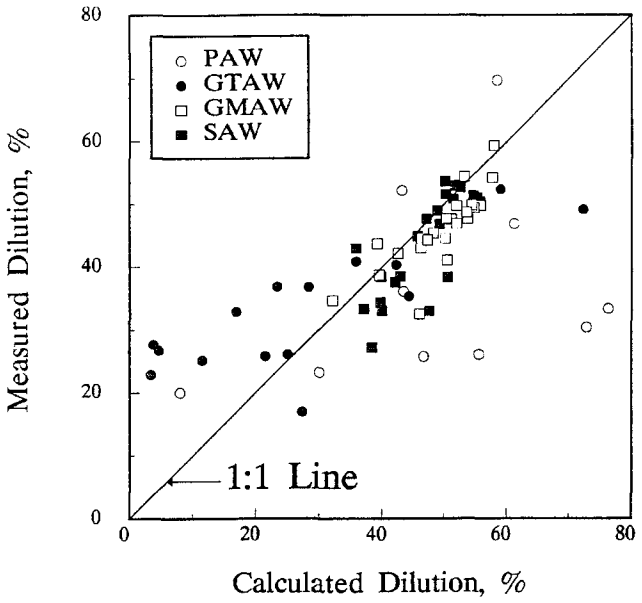

Fig. 4—Comparison of measured and calculated dilutions using Eq. [11] for each process evaluated.

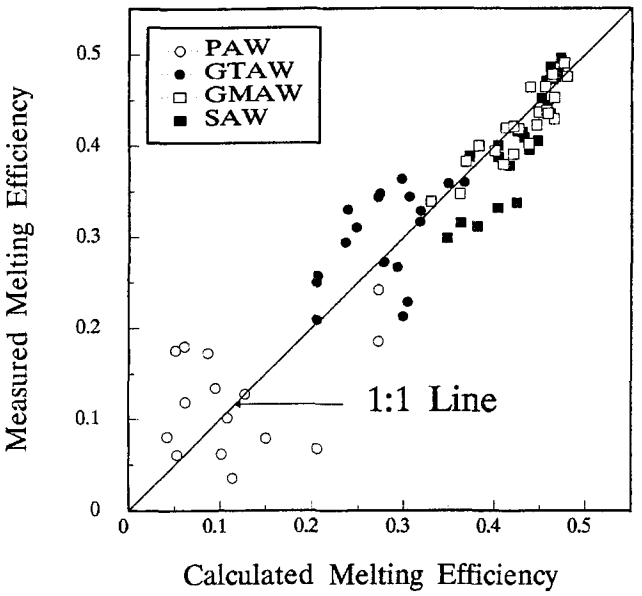

Fig. 5—Comparison of measured and calculated melting efficiencies using Eq. [5] for each process evaluated.

and substrate thermophysical properties. It should be noted that melting efficiency and dilution considerations are based only on the volumetric quantities of the deposited filler metal and melted substrate. The *shape* of the weld deposit need not be known to estimate these quantities.

It may be somewhat surprising to note that travel speed does not appear as a parameter in the dilution equation, since it is known from experience that increased travel speeds generally lead to increased dilution.[6,25] However, the relation between travel speed and dilution is readily apparent when the effect of travel speed on melting efficiency is considered *via* Eq. [5]. Melting efficiency increases with increasing travel speed. This increase in melting efficiency produces a concomitant increase in dilution *via* Eq. [11]. Therefore, the increase in dilution with travel speed is actually a direct result of the increased melting efficiency.

IV. RESULTS AND DISCUSSION

A. *Comparison of Measured and Calculated Dilution*

Figure 4 shows a comparison of measured and calculated dilutions for each process using Eq. [11], where the nominally constant values of arc efficiency for each process were used and melting efficiency values were determined by Eq. [5] with $A = 0.50$ and $B = 175$. As previously noted, $E_{fm} = 8.7$ J mm^{-3} and $E_s = 10.5$ J mm^{-3}. The agreement between experimentally measured and calculated dilution values shows a dependence on the process being compared. The agreement between measured and calculated dilution for the GMAW and SAW processes is reasonable, while the correlation begins to break down for the GTAW process. The correlation is poor for the PAW process.

This behavior results from the difficulty in accurately predicting melting efficiency at low values of $\eta_a VIS$ due to the exponential relation between η_m and $\eta_a VIS$. This is displayed in Figure 5, where the calculated melting efficiencies (using Eq. [5] with $A = 0.50$ and $B = 175$) and measured melting efficiencies of each process are plotted. The PAW and GTAW processes operate at relatively low values of $\eta_a VIS$ under the present set of conditions. This is a direct result of interactions between the arc efficiency and melting efficiency in which a low arc efficiency limits the maximum achievable melting efficiency. When the arc efficiency is low, the net power to the workpiece is low and it is difficult to reach high melting efficiencies (Eq. [5]). The arc efficiency also affects the melting efficiency by limiting the maximum travel speed which can be obtained. Operation at fast travel speeds requires high arc powers to compensate for the decreased time available for energy transfer to the workpiece by the heat source. If the maximum deliverable arc power is limited due to a low arc efficiency, then the maximum travel speed will also be limited and produce a further reduction in the melting efficiency. Thus, processes such as PAW and GTAW which exhibit low arc efficiencies will operate at relatively low values of $\eta_a VIS$ and low values of melting efficiency. However, in this region, small increases in arc power or travel speed promote large increases in the melting efficiency. As a result, melting efficiency is difficult to predict accurately from Eq. [5] in this range. The poor correlation of calculated and experimentally measured dilution for the PAW process is a result of the inability to accurately predict melting efficiency in this operating range (Figure 5). The GTAW process operates at slightly higher values of net arc power and travel speed, where the slope of the η_m *vs* $(\eta_a VIS/E\alpha\nu)$ curve begins to decrease. Thus, η_m can be predicted slightly better and the calculated dilution values are slightly closer to those observed experimentally. Finally, the GMAW and SAW processes operate at relatively high values of net arc power and travel speed, where η_m varies only slightly with $(\eta_a VIS/E\alpha\nu)$ and can be predicted quite accurately by Eq. [5] (Figure 5). Thus, the dilution values can also be predicted reasonably well (Figure 4).

Figure 6 shows the distribution of major alloying elements in a weld deposited by the GMAW process as determined by electron probe microanalysis. The parameters

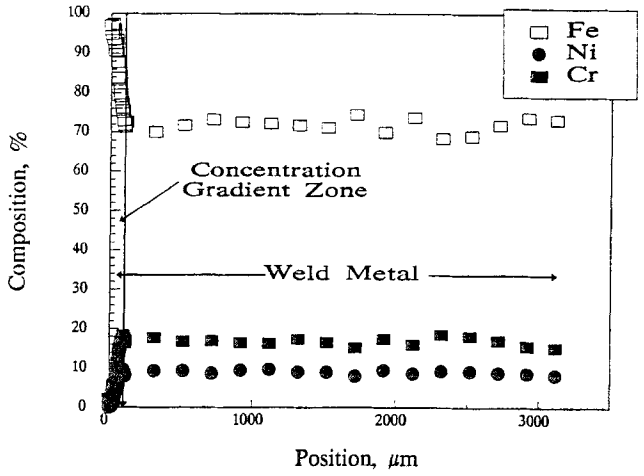

(a)

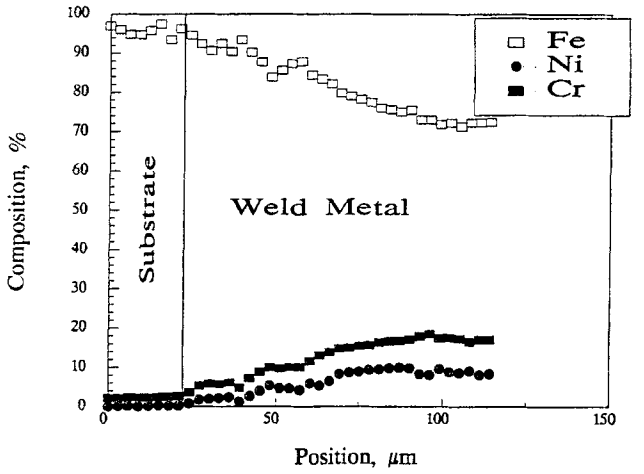

(b)

Fig. 6—Electron probe microanalysis profile of Fe, Cr, and Ni across a weld deposited by the GMAW process at 29 V, 245 A, and 16 mm/s travel speed. An overall plot of the data across the entire weld deposit; and (*b*) an expanded view near the fusion line.

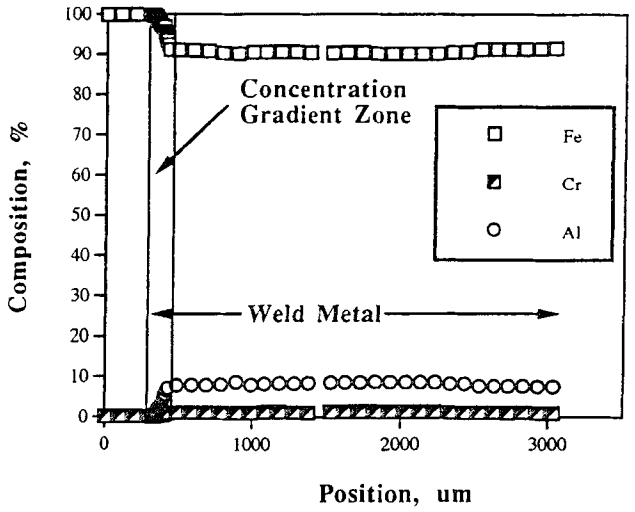

(a)

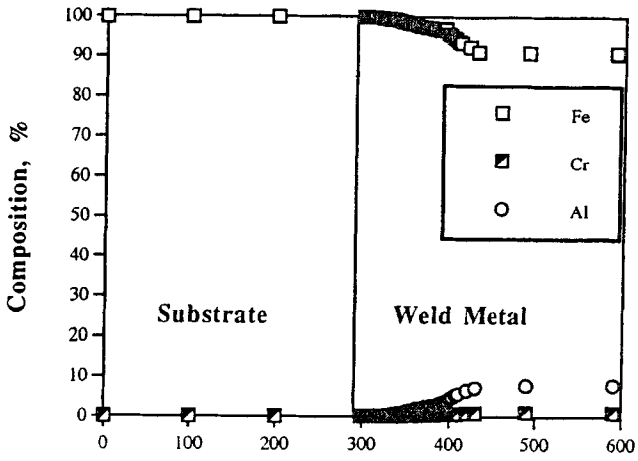

(b)

Fig. 7—Electron probe microanalysis profile of Fe, Cr, and Al across a weld deposited by the PAW process at 26.5 V, 300 A, and 3 mm/s travel speed. (*a*) An overall plot of the data across the entire weld deposit; and (*b*) an expanded view near the fusion line.

used to deposit the weld are noted in the figure caption. Figure 6(a) shows an overall plot of the data across the entire weld deposit, while Figure 6(b) shows an expanded view near the fusion line. These figures show that a concentration gradient exists near the fusion line over a distance of only ≈75 μm, after which the distribution of alloying elements is fairly uniform. Among the processes considered in this work, the GMAW (and SAW) process may be expected to provide the highest degree of mixing and most uniform distribution of elements due to metal transfer across the arc and subsequent injection into the molten pool. However, work at our laboratory on other alloy systems deposited by the PAW process, where no metal is transferred across the arc, has yielded results similar to those shown in Figure 6. As an example, Figure 7 shows the distribution of alloying elements in a weld prepared by depositing an Fe-Cr-Al powder filler alloy onto an A36 substrate using the PAW process. In this case, the concentration gradient is only ≈150 μm. In view of these data, it seems reasonable to assume the weld deposit will exhibit a fairly uniform distribution of alloying elements, and estimation of weld metal composition based on the geometric measurement of dilution (Eq. [1]) should represent the entire weld deposit composition reasonably well.

B. *Graphic Display of Processing Parameter Effects*

In many applications, it is often desirable to operate at high filler metal feed rates (deposition rates) for economic reasons, while maintaining low dilution levels for corrosion resistance or avoidance of undesirable phase formation. In this regard, it is useful to utilize the dilution equation to develop a graphical display which reveals the effect of processing parameters on dilution and provides an indication of the maximum filler metal feed rate, $V_{fm,\max}$, which can be achieved for a given level of melting power, $\eta_a \eta_m VI$.

Equation [11] is first solved in terms of the deposition rate, V_{fm}:

$$V_{fm} = \left(\frac{\gamma}{E_s + \gamma E_{fm}}\right) \eta_a \eta_m VI \qquad [12]$$

where

$$\gamma = \frac{1}{D} - 1 \qquad [13]$$

where D is the fraction (*i.e.*, not percent) dilution. Equations [12] and [13] indicate that, for a given filler metal/substrate combination (*i.e.*, E_{fm} and E_s fixed), a plot of filler metal feed rate (V_{fm}) against melting power ($\eta_a \eta_m VI$) will yield various slopes which depend only on the dilution. An indication of maximum filler metal feed rate for a given melting power can be considered to be reached when the dilution is reduced to zero and the filler metal does not adequately fuse to the substrate. This occurs when the volumetric melting rate of the substrate is zero, $V_s = 0$ (Eq. [6]). By setting $V_s = 0$ in the simple power balance of Eq. [8], the condition of maximum filler metal feed rate can be identified:

$$V_{fm,\max} = \left(\frac{1}{E_{fm}}\right) \eta_a \eta_m VI \qquad [14]$$

Equation [14] defines the condition where the filler metal feed rate is increased to the point where all the melting power would have to be used for melting the filler wire, in which case no melting power would remain to melt the substrate. This is the condition when the dilution is reduced to an undesirable level of zero. This is an obvious oversimplification of the problem, since it does not consider the relative rate of energy transport from the process to the filler metal and substrate. The condition is used here only to bound the limit for the maximum filler metal feed rate. Any filler metal feed rate utilized for a fixed melting power greater than that defined by Eq. [14] will certainly result in some incomplete melting of the substrate and/or filler metal. The exact value to the upper limit of filler metal feed rate which avoids partial melting (*i.e.*, incomplete fusion) between the filler metal and substrate cannot be determined with this approach.

The maximum filler metal feed rate defined here varies linearly with melting power by a line with slope ($1/E_{fm}$). Therefore, Eqs. [12] and [14] can be plotted on one diagram to reveal the maximum filler metal feed rate for a given melting power and the resultant dilution which will result from a given filler metal feed rate/melting power ratio. This concept is shown in the diagram in Figure 8. The filler metal feed rate (V_{fm}) is plotted as a function of the melting power ($\eta_a \eta_m VI$), and the slopes which correspond to various calculated dilution levels are plotted in 10 pct increments. Since the filler metal/substrate combination is fixed in this experiment, the slopes are determined only by the dilution. A boundary between an "inoperable range" and "operable range," as defined by Eq.[14], is also plotted. This line is also denoted as the 0 pct dilution line. Data for the SAW process are plotted and the measured values of dilution are shown in the data points for comparison to the calculated isodilution lines. As with Figure 4, the agreement is reasonable for the SAW process. This is to be expected since Figure 8 is simply a replot of the data presented in Figure 4. However, with this diagram, the effect of the processing parameters on dilution is readily apparent. For a fixed filler metal feed rate, the dilution increases with increasing melting power. In this case, the extra melting power cannot be absorbed by the filler metal if the filler metal feed rate is fixed, so the substrate absorbs the extra melting power

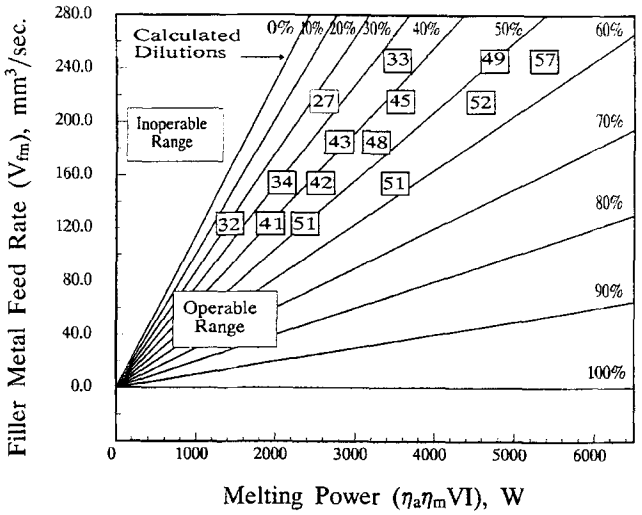

Fig. 8—Diagram showing the effect of processing parameters on dilution with experimental data for the SAW process.

which results in an increase in the volumetric melting rate of the substrate (V_s) and concomitant increase in dilution. Note that a filler metal feed rate of zero describes an autogenous weld which always has 100 pct dilution, as exhibited by the diagram. Conversely, for a given melting power, an increase in the filler metal feed rate results in a decrease in dilution. In this case, the filler metal consumes a larger portion of the total melting power and less energy is available to melt the substrate. As a result, the substrate volumetric melting rate decreases and dilution is reduced. When the filler metal feed rate is increased beyond the operable/inoperable boundary for a fixed melting power, where Eq. [14] is satisfied, the dilution reaches 0 pct (an undesirable condition). Thus, the effect of processing parameters on dilution and maximum filler metal feed rate is displayed on one diagram to facilitate parameter selection in applications where dilution and deposition rate are important.

The diagram also reveals the effect of differences in arc and melting efficiencies among the processes, which leads to differences in the ability of each process to achieve high filler metal feed rates under the present set of conditions. The consumable electrode processes exhibit the highest arc efficiency which, in turn, translates into high melting efficiency. By contrast, the nonconsumable electrode processes exhibit lower arc and melting efficiencies. Under conditions of equivalent arc power (VI), the amount of energy delivered to the workpiece for melting ($\eta_a \eta_m VI$) is reduced when the arc and melting efficiencies are lower. Considering Eq. [14] as a measure of maximum filler metal feed rate, it becomes apparent that high filler metal feed rates are favored by high thermal efficiency. Therefore, to avoid 0 pct dilution, higher arc powers (VI) or lower filler metal feed rates will be required for processes with low thermal efficiency in order to compensate for these energy losses. In regard to these considerations, the diagram can also be used to aid in the selection of the most suitable process for a given application. This is accomplished by plotting the data for all the processes on the diagram and comparing the processes in terms of the maximum achievable deposition rate. This comparison is made in Figure 9, where all the

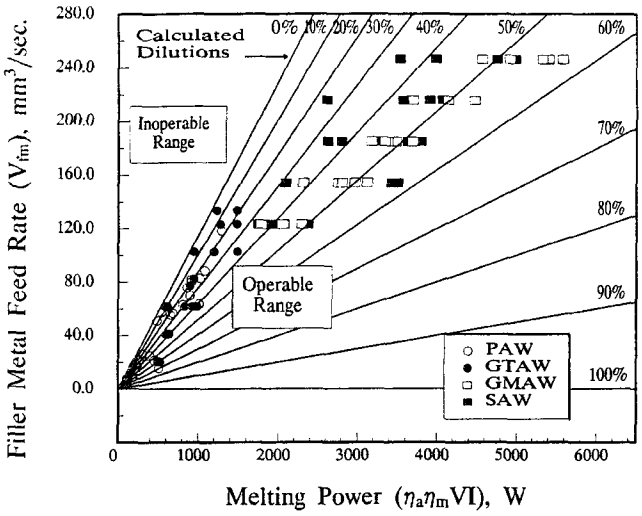

Fig. 9—Diagram showing the effect of processing parameters on dilution with experimental data for all processes.

data for the processes are plotted on one diagram and a distinct difference in terms of filler metal feed rate is observed between the consumable and nonconsumable electrode processes. (The experimental dilution data for the GMAW and SAW processes will be close to the calculated isodilution values, as illustrated by Figures 4 and 6. However, the dilution correlation for the PAW and GTAW processes is poor for reasons previously discussed and is plotted here only to reveal differences in maximum achievable filler metal feed rate.) With the consumable electrode processes operated under the present set of conditions, the thermal efficiency is high, which moves the operating conditions to high melting powers which, in turn, permit high deposition rates. The maximum deposition rate attainable in this work for the GMAW and SAW processes was 245 mm³/s. In contrast, the maximum deposition rate of nonconsumable electrode processes (PAW and GTAW) was limited to 120 to 130 mm³/s because the thermal efficiency is low.

C. *Significance and Limitations of Results*

The results presented here provide a straightforward approach to understanding the effects of processing variables on dilution in single pass arc welds. A main limitation to using the method quantitatively is the lack of data on the constants A and B in Eq. [5] to estimate melting efficiency. These values must be determined experimentally for a fixed substrate geometry. Considering that the functional dependence of η_m on arc power and travel speed is known, it may be possible to estimate these constants with relatively few experiments spanned over a broad parameter range and subsequently use them to estimate dilution over the entire range of parameters. In addition, it is not necessary to know values of E, α, or ν in Eq. [5] if the filler metal and substrate are fixed for a given application. In such cases, $E\alpha\nu$ is simply a constant and can be accounted for within the value of B. Last, it must be emphasized that the results presented here apply only to the simple single pass condition illustrated schematically in Figure 1. In most engineering applications, particularly cladding, multiple passes are required. Multiple passes will have the effect of increasing the substrate thickness which may affect A and B in Eq. [5]. If the substrate itself is thick enough to present three-dimensional heat flow conditions, where heat transfer is independent of substrate thickness, then A and B should not change with additional passes. Under cases where the substrate is relatively thin and two-dimensional heat flow exists, heat transfer will be dependent on the effective substrate thickness and additional passes are likely to affect A and B. In addition, an elevated interpass temperature is often maintained. This may be possible to handle experimentally by determining A and B with a substrate heated to the interpass temperature and reducing the enthalpy term E_s in Eq. [11] by an amount which is representative of the preheat temperature. Such details require further consideration before the approach can be utilized for these more general applications.

V. CONCLUSIONS

A study of dilution in single pass arc welds was conducted. Welds were deposited using type 308 austenitic stainless steel filler metal onto 6.4-mm-thick A36 carbon steel substrate using the PAW, GTAW, GMAW, and SAW processes. The dilution which results from a given set of processing parameters (V, I, S, and V_{fm}) can be estimated by

$$\text{Pct } D = [1 + \frac{V_{fm}E_s}{\eta_a\eta_m VI - E_{fm}V_{fm}}]^{-1} \times 100$$

where the arc efficiency, η_a, is nominally constant for a given process and melting efficiency, η_m, can be estimated by

$$\eta_m = A \exp\left(\frac{-B}{\eta_a VIS / E\alpha\nu}\right)$$

where A and B are experimentally determined constants. Under the present set of conditions, $A = 0.50$ and $B = 175$. Reasonable estimates of dilution are possible with these equations when the melting efficiency is relatively high and easy to accurately predict. The processing diagram proposed from the dilution equation facilitates selection of processing parameters in applications where dilution control is important.

NOMENCLATURE

A	constant in Eq. [5]
A_{fm}	cross-sectional area of deposited filler metal
A_s	cross-sectional area of melted substrate
B	constant in Eq. [5]
C_p	specific heat
D	dilution
d	width of weld
E	melting enthalpy
E_{fm}	melting enthalpy of filler metal
E_s	melting enthalpy of substrate
ΔH_f	latent heat of fusion
I	welding current
S	travel speed of heat source
V	voltage
V_{fm}	volumetric filler metal feed rate
V_s	volumetric melting rate of substrate

v_{fm}	melted filler metal volume
v_s	melted substrate volume
α	thermal diffusivity
η_a	arc efficiency
η_m	melting efficiency
γ	dilution parameter = $(1/D) - 1$
ν	kinematic viscosity at the melting point

ACKNOWLEDGMENTS

The authors gratefully acknowledge the support of this work by Ohio Edison, Potomac Electric Power Company, Pennsylvania Electric Energy Research Council, Dayton Power & Light, Public Service Electric & Gas, and Virginia Power. The assistance in metallographic preparation by A.O. Benscoter and in design and construction of the welding laboratory by L.R. Clements is also appreciated.

REFERENCES

1. C.L. Estes and P.W. Turner: *Weld. J.*, 1964, vol. 43 (12), pp. 541s-550s.
2. F. Ornath, J. Soudrey, B.Z. Weiss, and I. Minkoff: *Weld. J.*, 1981, vol. 60, pp. 227s-236s.
3. M.J. Cieslak and P.W. Fuerschbach: *Metall. Trans. B*, 1988, vol. 19B, pp. 319-29.
4. F.C. Hull: *Weld. J.*, 1973, vol. 52 (5), pp. 193s-203s.
5. R.S. Chandel: *Weld. Rev.*, 1987, No. 2, pp. 45-46.
6. Y.K. Oh, J.H. Devleation, and S.J. Chen: *Weld. J.*, 1990, vol. 69 (8), pp. 37-44.
7. T. Zacharia, A.H. Eraslan, and D.K. Aidun: *Weld. J.*, 1988, vol. 67 (1), pp. 18s-27s.
8. T. Zacharia, A.H. Eraslan, D.K. Aidun, and S.A. David: *Weld. J.*, 1988, vol. 67 (3), pp. 53s-62s.
9. T. Zacharia, A.H. Eraslan, D.K. Aidun, and S.A. David: *Metall. Trans. B*, 1989, vol. 20B, pp. 645-59.
10. T. Zacharia, S.A. David, and J.M. Vitek: *Metall. Trans. B*, 1991, vol. 22B, pp. 233-41.
11. J.N. DuPont and A.R. Marder: *Weld. J.*, 1995, vol. 74 (12), pp. 406s-416s.
12. W.H. Giedt, L.N. Tallerico, and P.W. Fuerschbach: *Weld. J.*, 1989, vol. 68 (1), pp. 28s-32s.
13. H.B. Smartt, J.A. Stewart, and C.J. Einerson: *Proc. ASM Int. Welding Congr.*, ASM, Metals Park, OH, 1985, ASM 8511-011, pp. 1-13.
14. A.D. Watkins, H.B. Smartt, and C.J. Einerson: *Proc. Recent Trends in Welding Science and Technology*, S.A. David and J.M. Vitek, eds., ASM INTERNATIONAL, Materials Park, OH, 1990, pp. 19-23.
15. D. Rosenthal: *Trans. ASME*, 1946, vol. 68, pp. 849-66.
16. A.A. Wells: *Weld. J.*, 1952, vol. 31 (5), pp. 263s-267s.
17. A. Okada: *J. Jpn. Weld. Soc.*, 1977, vol. 46 (2), pp. 53-61.
18. P.W. Fuerschbach and G.A. Knorovsky: *Weld. J.*, 1991, vol. 70 (11), pp. 287s-297s.
19. Y. Arata: *Plasma, Electron & Laser Beam Technology*, ASM, Metals Park, OH, 1986, p. 14.
20. D.T. Swift-Hook and A.E.F. Gick: *Weld. J.*, 1973, vol. 52 (11), pp. 492s-499s.
21. H.A. Fine and G.H. Geiger: *Handbook on Material and Energy Balance Calculations in Metallurgical Processes*, AIME, Warrendale, PA, 1979, p. 431.
22. C.F. Lucks and H.W. Deem: *Thermal Properties of Thirteen Metals*, STP No. 227, ASTM, Philadelphia, PA, 1958.
23. E.A. Brandes: *Smithells Metals Reference Book*, 6th ed., Butterworth and Co., London, 1983.
24. T.F.G. Grey, J. Spence, and T.H. North: *Rational Welding Design*, Newnes-Butterworths, London, 1975.
25. S.G. Forsberg: *Weld. J.*, 1985, vol. 64 (8), pp. 41-48.